Oil & Gas Science and Technology – Rev. IFP Energies nouvelles **76**, 14 (2021)

https://doi.org/10.2516/ogst/2020097

Available online at:
ogst.ifpenergiesnouvelles.fr

REGULAR ARTICLE OPEN ACCESS

Cyclic methane hydrate production stimulated with CO_2 and N_2

Zhizeng Xia[1,*], Jian Hou[2], Xuewu Wang[1], Xiaodong Dai[1], and Mingtao Liu[3]

[1] Shengli College, China University of Petroleum, Dongying City, Shandong Province 257061, PR China
[2] School of Petroleum Engineering, China University of Petroleum (East China), Qingdao City 266580, PR China
[3] Twelfth Oil Production Plant, Petro China Changqing Oilfield Branch, Qingyang City 744505, PR China

Received: 26 September 2020 / Accepted: 9 December 2020

Abstract. The cyclic methane hydrate production method was proposed with CO_2 and N_2 mixture stimulation. The cyclic production model was established based on actual hydrate reservoir parameters, accordingly, the production characteristics were analyzed, and a sensitivity analysis was conducted. The results show the following: (1) The depressurization mechanism is dominant in the cyclic production. CH_4 production and CH_4 hydrate dissociation can be greatly enhanced because the cyclic process can effectively reduce the partial pressure of CH_4 (gas phase). However, there is a limited effect for CO_2 storage. (2) Heat supply is essential for continuous hydrate dissociation. The CH_4 hydrate dissociation degree is the highest in the near-wellbore area; in addition, the fluid porosity and effective permeability are significantly improved, and the reservoir temperature is obviously decreased. (3) The initial CH_4 hydrate saturation, absolute permeability, intrinsic CO_2 hydrate formation kinetic constant, injection time and production time can significantly influence the production performance of the natural gas hydrate reservoir.

1 Introduction

Natural gas hydrates (mainly methane hydrates) are crystalline solids stabilized under low-temperature and high-pressure environments, which have been considered a potential energy supply since the mid-1960s due to their wide distribution and enormous reserves [1]. Therefore, the effective development of hydrate reservoirs (*i.e.*, the methane recovery) is of great significance.

Currently, depressurization, heat stimulation, chemical inhibitor stimulation and gas exchange (CO_2) are the most investigated methods for hydrate reservoir development [2]. Among these methods, the depressurization method is acknowledged as the most potential one due to its simplicity and efficiency. Many studies in the depressurization method have been conducted, such as sensitivity analysis of laboratory-scale parameters [3], heat transfer behavior [4], hydraulic fracturing enhanced depressurization [5], decreasing bottom-hole pressure [6], hydrate production trials in the Mallik area [7], Eastern Nankai Trough [8] and South China Sea [9], and relevant simulation studies [10–12].

The gas exchange method was initially proposed by Ohgaki *et al.* [13]. When the environment temperature was lower than 10 °C (283 K), the CO_2 hydrate was more stable than the CH_4 hydrate (Fig. 1). The CH_4 hydrate will dissociate, and the CO_2 hydrate will form if the reservoir condition falls into the shadow area in Figure 1. Therefore, CO_2 injection into hydrate reservoirs can enhance CH_4 recovery and sequester CO_2 (the well-known greenhouse gas) under a suitable P-T range. This is the main reason why the gas exchange method has received special attention in recent years. Lee *et al.* [14] investigated the influence of the CO_2 addition on $CH_4 + C_3H_8$ hydrates from thermodynamic, microscopic and kinetic aspects, and found high replacement degree at the high CO_2 pressure. Gharasoo *et al.* [15] developed a model of CO_2 injection into a gas-hydrate-filled pressure vessel, and evaluated the effective gas hydrate dissociation rate into gas and water by fitting the experimental results. Shagapov *et al.* [16] developed the mathematical model of the warm CO_2 injection into a CH_4-saturated hydrate reservoir and concluded that the CO_2 hydrate formation heat had a great impact on the CH_4 hydrate dissociation rate. Khasanov *et al.* [17] also developed a similar mathematical model of liquid CO_2 injection into the hydrate reservoir and analyzed four different regimes during the process. All these investigations showed the feasibility of the methane recovery from hydrate reservoirs through CO_2 injection.

However, the effect of pure CO_2 injection into the hydrate reservoir may be quite limited, and experimental studies have shown that the existence of N_2 in the CO_2 stream can improve the sweeping region and recovery efficiency. Koh *et al.* [18] investigated the fluid flow characteristics and exchange mechanisms of continuous CO_2/N_2

* Corresponding author: z.xia_cn@outlook.com

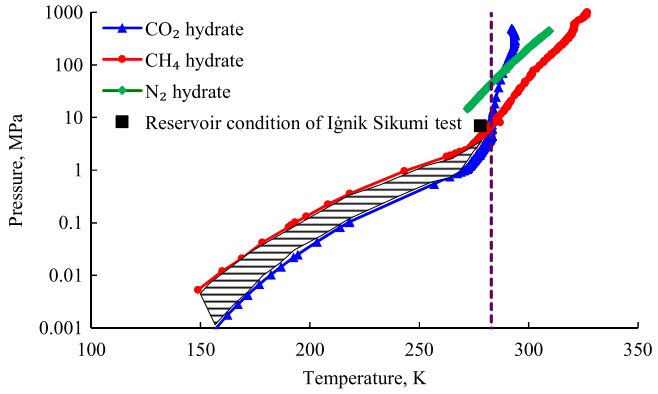

Fig. 1. Pressure-temperature phase equilibrium curves of the CH_4, CO_2 and N_2 hydrates (data from Sloan [1]).

injection into a one-dimensional high-pressure reactor containing the hydrate, and they found that the exchange efficiency was inversely proportional to the gas injection rate. Yang *et al.* [19] investigated the dissociation of the CH_4 hydrate stimulated with flue gas flooding through a sand pack model, and they concluded that the flue gas injection was potential for hydrate production and CO_2 sequestration. Li *et al.* [20] investigated the fracture-filled CH_4 hydrate dissociation by CO_2 and CO_2/N_2 injection, respectively, and they found that the presence of N_2 could enhance the final accumulative methane recovery ratio and exchange rate. In addition to N_2, Sun *et al.* [21] also studied the hydrate dissociation using the CO_2/H_2 mixture injection, and they observed good CH_4 hydrate recovery ratio and CO_2 storage capability.

Although the gas exchange method is promising, the low production rate or efficiency is the main disadvantage of this method. Merey *et al.* [22] reviewed the CH_4–CO_2 exchange studies and pointed out that the combination of depressurization and gas exchange was promising for hydrate reservoir development. Okwananke *et al.* [23] experimentally studied the enhanced-depressurization for CH_4 hydrate dissociation by injection of compressed air and nitrogen, and they found that the CH_4 hydrate was quickly dissociated and concluded that the gas injection was a potential approach to improve conventional depressurization method for the hydrate reservoir development. Based on extensive experimental and numerical investigations, the Iğnik Sikumi Field production trial was carried out to assess the CH_4 production potential with CO_2/N_2 stimulation in 2012. In this production trial, a huff and puff method was used which was a combination of depressurization and gas exchange, and the "bulk exchange" may have occurred [24].

To investigate the possibility of simultaneous CH_4 production and CO_2 sequestration in a field scenario, this paper proposed a cyclic CH_4 hydrate production method stimulated by CO_2 and N_2 mixture based on the production trial mentioned above. An actual-parameter based simulation model was established, the CH_4 hydrate production characteristics were evaluated, and a sensitivity analysis was carried out.

2 Model description

2.1 Production method

The injected gas in this paper is a mixture of CO_2 and N_2, and the existence of a N_2 hydrate is ignored because it is difficult to form under typical hydrate reservoir conditions (Fig. 1). The cyclic production scheme [25] is adopted to conduct this research, which is widely used in the heavy oil production by high-temperature steam stimulation in the petroleum industry. The whole production process is composed of several production cycles and each production cycle includes the injection stage, the soaking stage and the production stage. The well is opened in the injection and production stage, and during the soaking stage, the well is shut in in order that the injected gas and pressure disturbance can originate in the depth of the reservoir.

2.2 Simulator selection

The methane recovery from the hydrate reservoir is a complicated process involving phase transition, heat and mass transfer, multi-phase flow, etc. Numerical simulation is an effective way to investigate the possible hydrate production behaviors and several codes/simulators have been used to carry out relevant analyses. In this paper, the *CMG-STARS* [26] was selected to conduct the simulation study. This simulator was used to simulate hydrate reservoir production in the Mount Elbert area [27], and it obtained long-term production characteristics similar to other tested simulators. In addition, it has also been used for sensitivity studies of CH_4 hydrate production [28], economic studies [29], gas production behavior [30], and CO_2 hydrate formation in depleted gas reservoirs [31]. The base model was established using *CMG-STARS* by referring to the reservoir and operation parameters of the Iğnik Sikumi Field production trial.

2.3 Fundamentals

2.3.1 Mass and energy conservation

Assuming that the hydrates in the reservoir are pure CH_4 hydrates, the system is composed of the immobile phase (hydrate phase) and the mobile phases (aqueous and gas phases), and the flows of the gas and aqueous phases follow Darcy's law. The relationships among the components and phases in this study are shown in Table 1. For each single cell, the spatially discretized conservation equations of each component and the energy are shown in equations (1), (2) and (3), respectively.

For the conservation of the flowing component i (*i.e.*, CH_4, CO_2, N_2 or H_2O):

$$\frac{\partial}{\partial t}\left[V_f(\rho_A S_A^e w_i + \rho_G S_G^e y_i)\right] = \sum_{n=1}^{n_f}\left[\left(\frac{A}{l}\right)^e k^e\left(\frac{k_{rA}}{\mu_A}\rho_A w_i \Delta p_A + \frac{k_{rG}}{\mu_G}\rho_G y_i \Delta p_G\right)\right] + V_b\sum_{n=1}^{n_t}\left(s_{ni}^{'} - s_{ni}\right)r_n + q_i, \quad (1)$$

Table 1. Relationships among the components and phases.

	CH_4	CO_2	N_2	H_2O	$CH_4{\cdot}NH_2O$	$CO_2{\cdot}NH_2O$
Gas phase	√	√	√	√		
Aqueous phase				√		
Hydrate phase (solid)					√	√

Note: the check indicates that the component exists in this phase; N is the hydration number, which is set to 5.75 for the CH_4 hydrate and CO_2 hydrate.

where V_f is the volume occupied by the mobile phases; V_b is the apparent volume of the cell; ρ_A and ρ_G are the density of the aqueous and gas phases, respectively; w_i and y_i are the mass percent of component i in the aqueous and gas phases, respectively; n_f is the number of neighboring cell faces; $\left(\frac{A}{l}\right)^e$ is the ratio of the effective area and distance between interfaces; k^e is the effective permeability at the interface; p_A and p_G are the pressure of the aqueous and gas phases, respectively; n_t is the number of chemical reactions; s_{ni} and s_{ni} are the product and reactant stoichiometric coefficients of component i, respectively; r_n is the volumetric reaction rate; and q_i is the mass source/sink from the injection/production wells.

For the conservation of the solid component i (*i.e.*, $CH_4{\cdot}NH_2O$ or $CO_2{\cdot}NH_2O$):

$$\frac{\partial}{\partial t}[V_v c_i] = V_b \sum_{n=1}^{n_f} \left(s_{ni}^{'} - s_{ni}\right) r_n, \tag{2}$$

where V_v is the volume occupied by the mobile and immobile phases and c_i is the volumetric concentration of the solid component i.

For energy conservation:

$$\begin{aligned}\frac{\partial}{\partial t}\left[V_f(\rho_A S_A^e U_A + \rho_G S_G^e U_G) + V_v c_S U_S + V_r U_r\right] \\ = \sum_{n=1}^{n_f}\left[\left(\frac{A}{l}\right)^e k^e\left(\frac{k_{rA}}{\mu_A}\rho_A H_A \Delta p_A + \frac{k_{rG}}{\mu_G}\rho_G H_G \Delta p_G\right)\right] \\ + \sum_{n=1}^{n_f}\left(\frac{A}{l}\right)^e \lambda^e \Delta T + V_b \sum_{n=1}^{n_r} H_{rn} r_n + q_e,\end{aligned} \tag{3}$$

where V_r is the rock volume (solid inert matrix, rock grains); c_S is the total solid concentration; U_r is the internal energy per rock volume; U_A, U_G and U_S are the internal energy of the aqueous, gas and solid phases, respectively; H_A, H_G and H_{rn} are the enthalpy of the aqueous phase, gas phases and reaction n, respectively; λ^e is the effective thermal conductivity at the interface; T is the temperature; and q_e is the heat source/sink from the injection/production wells.

2.3.2 Permeability model

When the hydrate exists, the fluid phase permeability in the porous medium will decrease [32]. Currently, there are two methods to treat the permeability variation in the presence of the hydrate [33], namely, the variable absolute permeability method and the constant absolute permeability method. For the first method, the reservoir absolute permeability is modeled as a function of the hydrate saturation; in addition, the mobile phase relative permeability changes with the effective phase saturation. In the second method, the reservoir absolute permeability is constant, while the mobile phase relative permeability changes with the actual phase saturation. We adopted the first method to conduct our research. The definitions of the fluid phase permeability, effective phase saturation and actual phase saturation are shown in equations (4), (5) and (6), respectively:

$$k_\beta = k_a k_{r\beta}, \tag{4}$$

where k_β is the effective permeability of phase β; k_a is the absolute permeability of the hydrate reservoir; and $k_{r\beta}$ is the relative permeability of phase β:

$$S_\beta^e = \frac{V_\beta}{V_f}, \tag{5}$$

where $S^e{}_\beta$ is the effective saturation of phase β.

$$S_\beta = \frac{V_\beta}{V_v}, \tag{6}$$

where S_β is the actual saturation of phase β.

(1) Absolute permeability model (Carman-Kozeny-type formula)

$$k_a = k_{a0}\left(\frac{\varphi_f}{\varphi}\right)^m \left(\frac{1-\varphi}{1-\varphi_f}\right)^2, \tag{7}$$

where k_{a0} is the reservoir absolute permeability without the existence of the gas hydrate; φ and φ_f are the reservoir porosity and fluid porosity, respectively; and m is the model parameter, which is set to 4.3413 by transforming the Civan's permeability-porosity relationship from Anderson *et al.* [34].

(2) Relative permeability model

The flows of the mobile phases follow Darcy's law, and the relative permeability models are shown in equation (8):

$$\begin{aligned} k_{rA} &= \left[\frac{S_A^e - S_{irA}}{1 - S_{irA}}\right]^{n_A} \\ k_{rG} &= \left[\frac{S_G^e - S_{irG}}{1 - S_{irA}}\right]^{n_G}, \end{aligned} \tag{8}$$

where k_{rA} and k_{rG} are the relative permeability of the aqueous and gas phases, respectively; S_{irA} and S_{irG} are the irreducible aqueous and gas saturation, respectively;

Table 2. Intrinsic dissociation/formation rate constants of the CH_4/CO_2 hydrate.

		CH_4 hydrate	CO_2 hydrate
k_0, mol m^{-2} Pa^{-1} s^{-1}	Dissociation	3.60×10^4 [41]	1.83×10^8 [42]
	Formation	2.90×10^{-3} [40]	3.50×10^{-4} [40]

n_A is the model parameter, which is set to 5.04 [35]; and n_G is the model parameter, which is set to 3.16 [35].

2.3.3 Capillary pressure model

The capillary pressure between the gas phase and the aqueous phase is shown in equation (9):

$$p_c = -p_{c0}\left[\left(\frac{S_A^e - S_{irA}}{1 - S_{irA}}\right)^{-1/\lambda} - 1\right]^{1-\lambda}, \quad (9)$$

where p_c is the capillary pressure; p_{c0} is the model parameter, which is set to 10^4 Pa [35]; and λ is the model parameter, which is set to 0.77437 [35].

2.3.4 CH_4/CO_2 hydrate dissociation/formation model

Two chemical reactions shown in equations (10) and (11) are considered:

$$CH_4 \cdot NH_2O \leftrightarrow CH_4 + NH_2O + \Delta H_1, \quad (10)$$

$$CO_2 \cdot NH_2O \leftrightarrow CO_2 + NH_2O + \Delta H_2. \quad (11)$$

where ΔH_1 and ΔH_2 are the enthalpy of CH_4 hydrate dissociation/formation and CO_2 hydrate dissociation/formation, which are set to 56.84 kJ mol^{-1} [36] and 65.22 kJ mol^{-1} [36], respectively.

(1) Hydrate dissociation rate model

In 1987, Kim and Bishnoi proposed the widely used CH_4 hydrate dissociation kinetic model based on experimental results [37, 38]. In their model, the dissociation rate was proportional to the hydrate particle surface area or dissociation area and to the difference in the methane fugacity at the equilibrium and dissociation pressures. The fugacity can be approximated with an equivalent pressure when setting the fugacity coefficient equal to 1.0 [39].

We assume that both the dissociation and formation of the CH_4 hydrate and CO_2 hydrate follow the Kim-Bishnoi model. The expression of the CH_4/CO_2 hydrate dissociation rate can be expressed as follows: [40]

$$\frac{dc_{Hyd}}{dt} = \left(\frac{k_d^0 A_{HS}}{\rho_w \rho_h}\right)\left(\varphi^2 \rho_w \rho_h S_A S_H p_e\right) \exp\left(-\frac{\Delta E_d}{RT}\right)\left(1 - \frac{y}{K(p,T)}\right), \quad (12)$$

where c_{Hyd} is the mole quantity of the CH_4/CO_2 hydrate per unit volume; k_d^0 is the intrinsic dissociation rate constant of CH_4/CO_2 hydrate (Tab. 2); A_{HS} is the reaction specific area, which is 750,000 m^2/m^3 (*i.e.*, hydrate particles are assumed to be regular spheres with a diameter of 8 μm [41]); ρ_w is the density of the aqueous phase, 1000 kg/m^3; ρ_h is the density of the CH_4 hydrate or CO_2 hydrate, 919.7 kg/m^3 or 1100 kg/m^3 [40]; ΔE_d is the activation energy of the dissociation reaction, which is 81 kJ/mol [41] and 102.88 kJ/mol [42] for the CH_4 hydrate and CO_2 hydrate, respectively; R is the gas universal constant; p_e is the equilibrium pressure; y is the mole fraction of CH_4/CO_2 in gas phase; and K is the equilibrium ratio, as follows:

Table 3. Model parameters of the equilibrium ratio.

	CH_4 hydrate	CO_2 hydrate
a_1, Pa	2.6204×10^{11}	1.0861×10^{11}
a_2, °C	−2963.891	−2312.9531
a_3, °C	−160.42403	−125.86524

$$K = \left(\frac{a_1}{p_g}\right)\exp\left(\frac{a_2}{T - a_3}\right), \quad (13)$$

where p_g is the gas phase pressure; a_1, a_2 and a_3 are model parameters, and they are calculated based on the experimental results of Adisasmito *et al.* [43] (Tab. 3), where the average fitting error is 0.46% and 0.39% for the CH_4 hydrate and CO_2 hydrate, respectively.

(2) Hydrate formation rate model

Similar to equation (12), the expression of the CH_4/CO_2 hydrate formation rate (including nucleation and growth) can be expressed as equations (14) and (15).

For the hydrate nucleation process:

$$\frac{dc_{Hyd}}{dt} = \left(\frac{k_f^0 A_{HS}}{\rho_w}\right)\left(\varphi \rho_w S_A p_e\right) \exp\left(-\frac{\Delta E_f}{RT}\right)\left(1 - \frac{y}{K(p,T)}\right). \quad (14)$$

For the hydrate growth process:

$$\frac{dc_{Hyd}}{dt} = \left(\frac{k_f^0 A_{HS}}{\rho_w \rho_h}\right)\left(\varphi^2 S_A S_H \rho_w \rho_h p_e\right) p_e \times \exp\left(-\frac{\Delta E_f}{RT}\right)\left(1 - \frac{y}{K(p,T)}\right), \quad (15)$$

where k_f^0 is the intrinsic formation rate constant of the CH_4/CO_2 hydrate (Tab. 2), and ΔE_f is the activation energy of the formation reaction, which is assumed to be equal to that of the dissociation reaction for the CH_4 hydrate or CO_2 hydrate.

Table 4. Reservoir parameters of the HBL.

Parameter and unit	Value	Parameter and unit	Value
Absolute permeability, mD	1000	Irreducible aqueous saturation	0.10
Reservoir thickness, m	9	Irreducible gas saturation	0.00
Reservoir porosity	0.40	Initial reservoir pressure, MPa	6.9
Initial CH_4 hydrate saturation	0.72	Initial reservoir temperature, °C	5
Initial aqueous saturation	0.28		

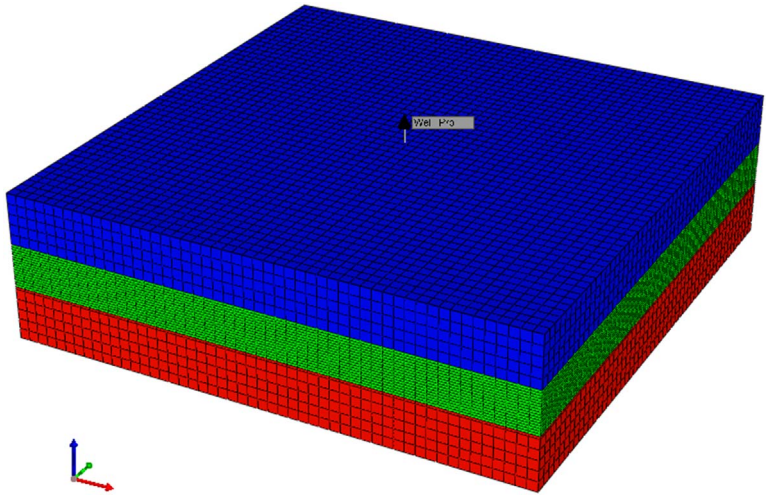

Fig. 2. Sketch of the base model.

Table 5. Operation parameters.

Stage	Parameter and unit	Value	Stage	Parameter and unit	Value
Injection stage	Time duration, d	15	Soaking stage	Time duration, d	5
	Maximum gas injection rate, m^3/d	500	Production stage	Time duration, d	30
	Injected gas temperature, °C	100		BHP, MPa	4.5
	Maximum BHP, MPa	10			

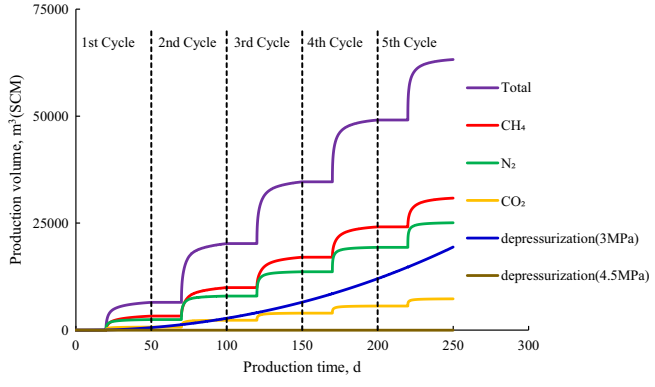

Fig. 3. Gas production volume of the base model.

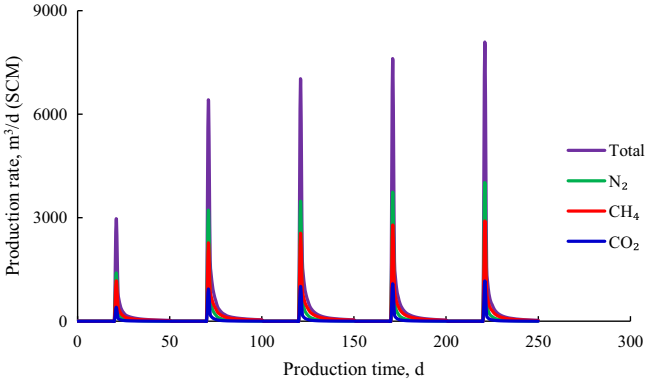

Fig. 4. Gas production rate of the base model.

Table 6. CH_4 production volume in each cycle.

Cycle number	1st	2nd	3rd	4th	5th
CH_4 production, m^3	3302.8	6647.8	7101.0	7086.1	6718.5
Total gas production, m^3	6509.8	13 735.3	14 428.6	14 444.4	14 132.0
CH_4 percent in the total gas production, %	50.7	48.4	49.2	49.1	47.5

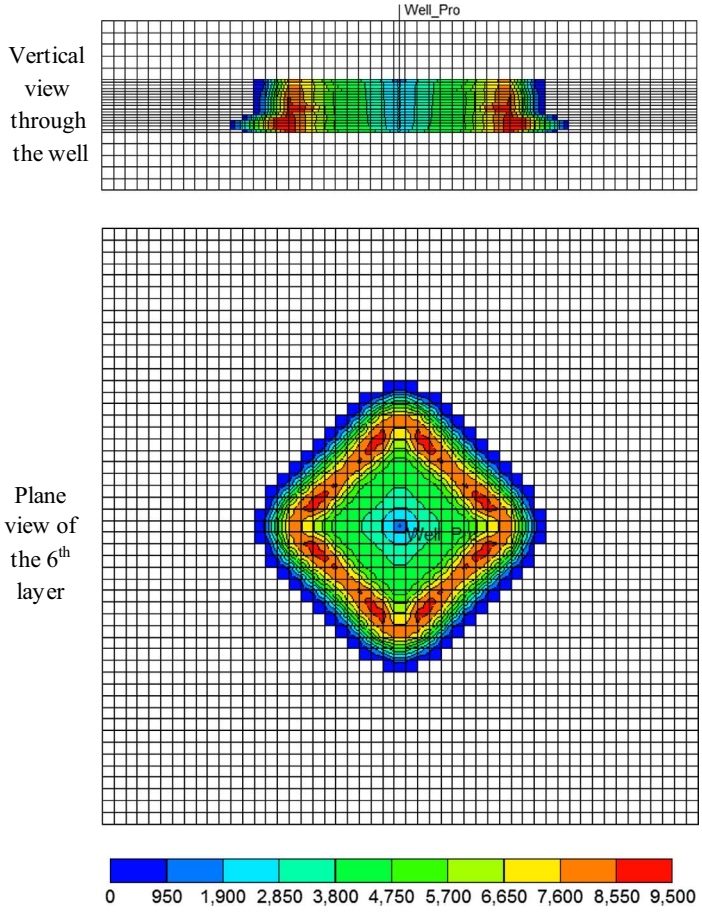

Fig. 5. CH_4 partial pressure in the gas phase at the end of the injection stage of the 1st cycle (kPa).

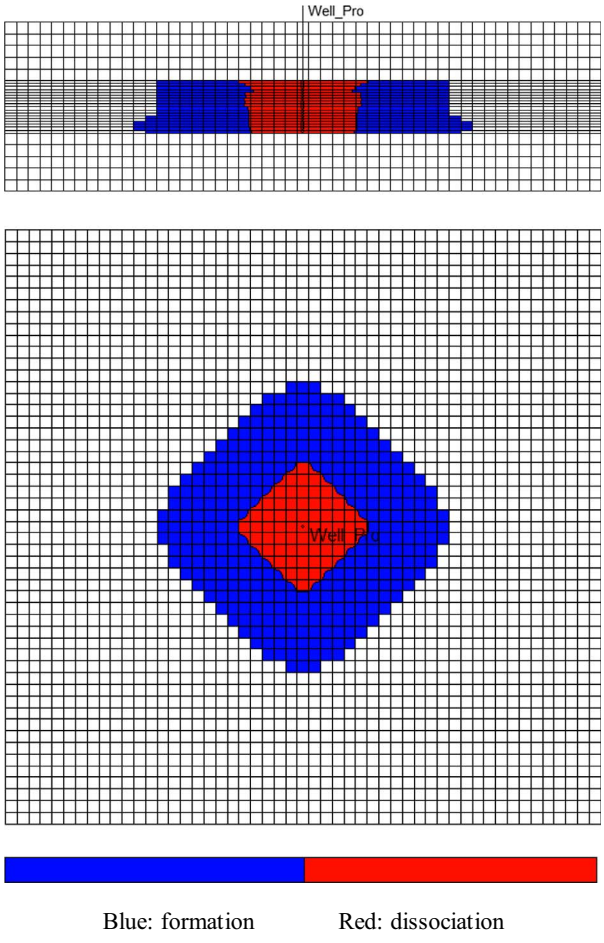

Fig. 6. CH_4 hydrate formation and dissociation area at the end of the injection stage of the 1st cycle.

2.4 Base model

2.4.1 Reservoir parameters

As shown in Table 4, the model is established based on the reservoir parameters of "C–1 sand" [24, 44] (one of four separate hydrate-bearing units according to the Ignik Sikumi well-log data) and is composed of the overlying layer (impermeable), the Hydrate-Bearing Layer (HBL), and the bottom layer (impermeable) with thicknesses of 10 m, 9 m and 10 m, respectively. The model size is 102 m × 102 m × 29 m with a grid division of 51 × 51 × 28. At the initial CH_4 hydrate saturation of 0.72 (corresponding to the concentration of 5539 mol/m^3 in the base model), the effective permeability and fluid porosity of the HBL are 1.82 mD and 11.2%, respectively. The sketch of the base model are shown in Figure 2.

2.4.2 Operation parameters

The hydrate reservoir is produced by cyclic gas injection with a composition of 22.5 mol% CO_2 and 77.5 mol% N_2. The maximum Bottom-Hole Pressure (BHP) was maintained lower than the formation breakdown pressure (10 MPa) for operation safety during the gas injection stage. A total of 5 production cycles (250 d) were conducted. The main operation parameters are shown in Table 5.

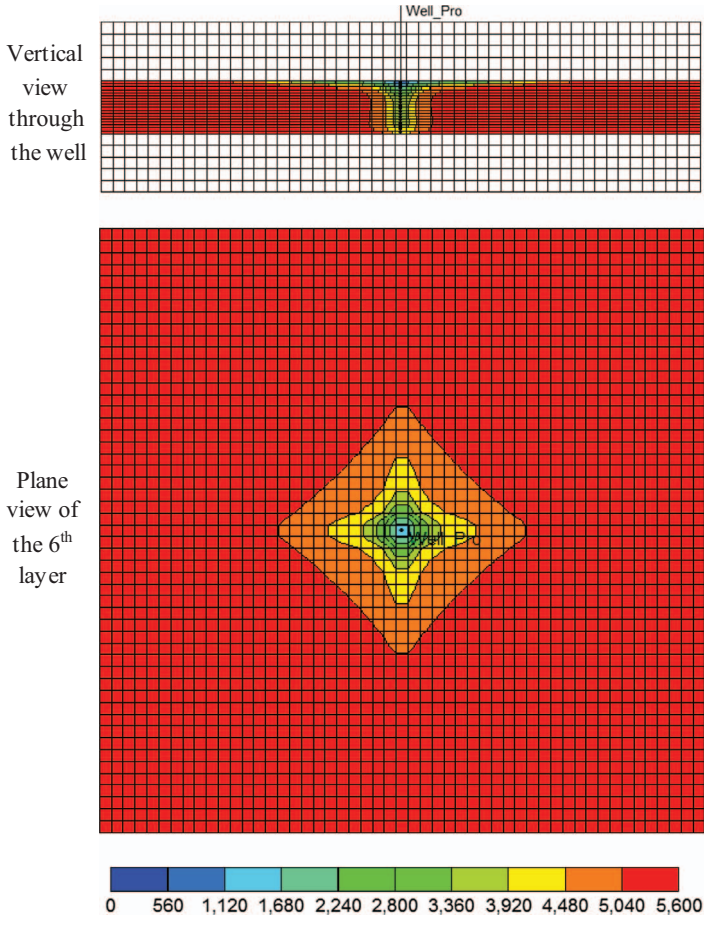

Fig. 7. CH_4 hydrate concentration at the end of the simulation (mol/m^3).

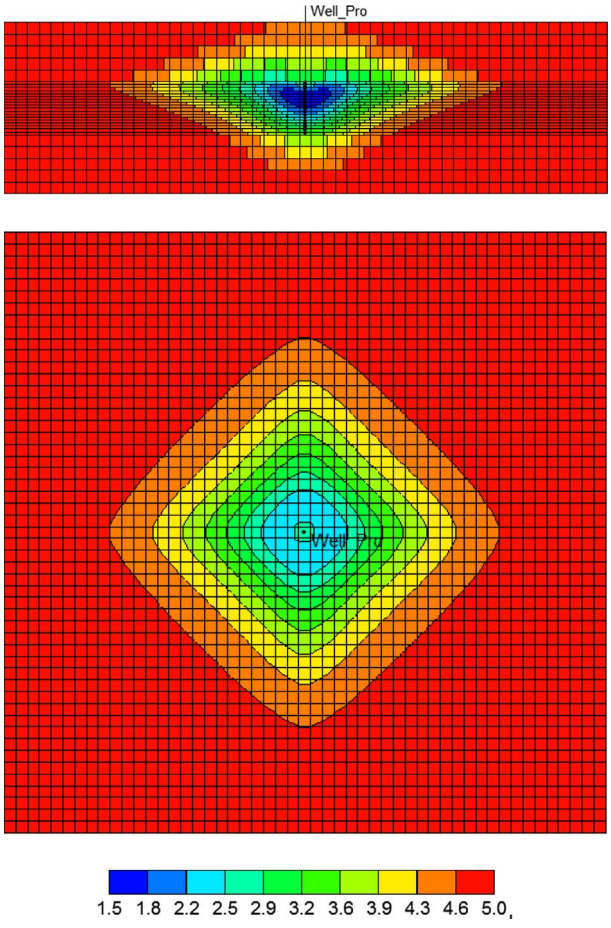

Fig. 8. Temperature distribution at the end of the simulation (°C).

3 Results and discussion

3.1 Production characteristics

Figures 3 and 4 show the production volume and the production rate of each gas component, respectively. The gas production rate changes periodically, where the highest production rate occurs at the beginning in each cycle, because the diving force (*i.e.* the production pressure difference) is the largest at this time. A total of 63 250 m^3 (SCM) of gas is produced at the end of the simulation, where CH_4 accounts for 48.78%. The peak gas production rate of each production cycle increases with the increase of the cycle number, where the highest value reaches 8090 m^3/d. From Table 6, the total production volume of CH_4 remains almost the same except the first cycle, and the percent of the CH_4 in the total gas production accounts for about 50% in each cycle. At a constant BHP of 4.5 MPa, if no gas was injected into the hydrate reservoir, there would be no CH_4 production (the curve labelled with "depressurization (4.5 MPa)" in Fig. 3) when the BHP maintains at 4.5 MPa. This is because it is higher than the corresponding equilibrium pressure of the CH_4 hydrate (4.34 MPa) at the reservoir condition. Besides, the total CH_4 produced by the cyclic production method is 50% more than that by the depressurization method at the BHP of 3 MPa (the curve labelled with "depressurization (3 MPa)" in Fig. 3). This shows the production potential of the cyclic production. Depressurization method obtains the CH_4 production by lowering the reservoir pressure which is economical and simple. However, for low-pressure hydrate reservoirs, the minimum BHP usually cannot be smaller than 2.75 MPa to avoid potential ice formation, and thus the available pressure-reduction space is quite limited, which affects the production. Under this situation, using the cyclic production can enhance CH_4 production.

The injected CO_2 and N_2 can cause the partial pressure to change in the gas component and thus affect the stability of the gas hydrate. For the CH_4 hydrate, using the 1st cycle as an example, the partial pressure of CH_4 in the gas phase and the area below/above the corresponding equilibrium pressure at the end of the injection stage are shown in Figures 5 and 6, respectively. From Figure 5, the average radius of pressure propagation into the hydrate reservoir

Table 7. CO_2 storage percent at the end of each cycle.

Cycle number	1st	2nd	3rd	4th	5th
CO_2 storage percent, %	9.83	6.89	5.04	4.13	3.46

Note: The CO_2 storage percent is defined as the ratio of CO_2 remaining in the reservoir to the injected CO_2.

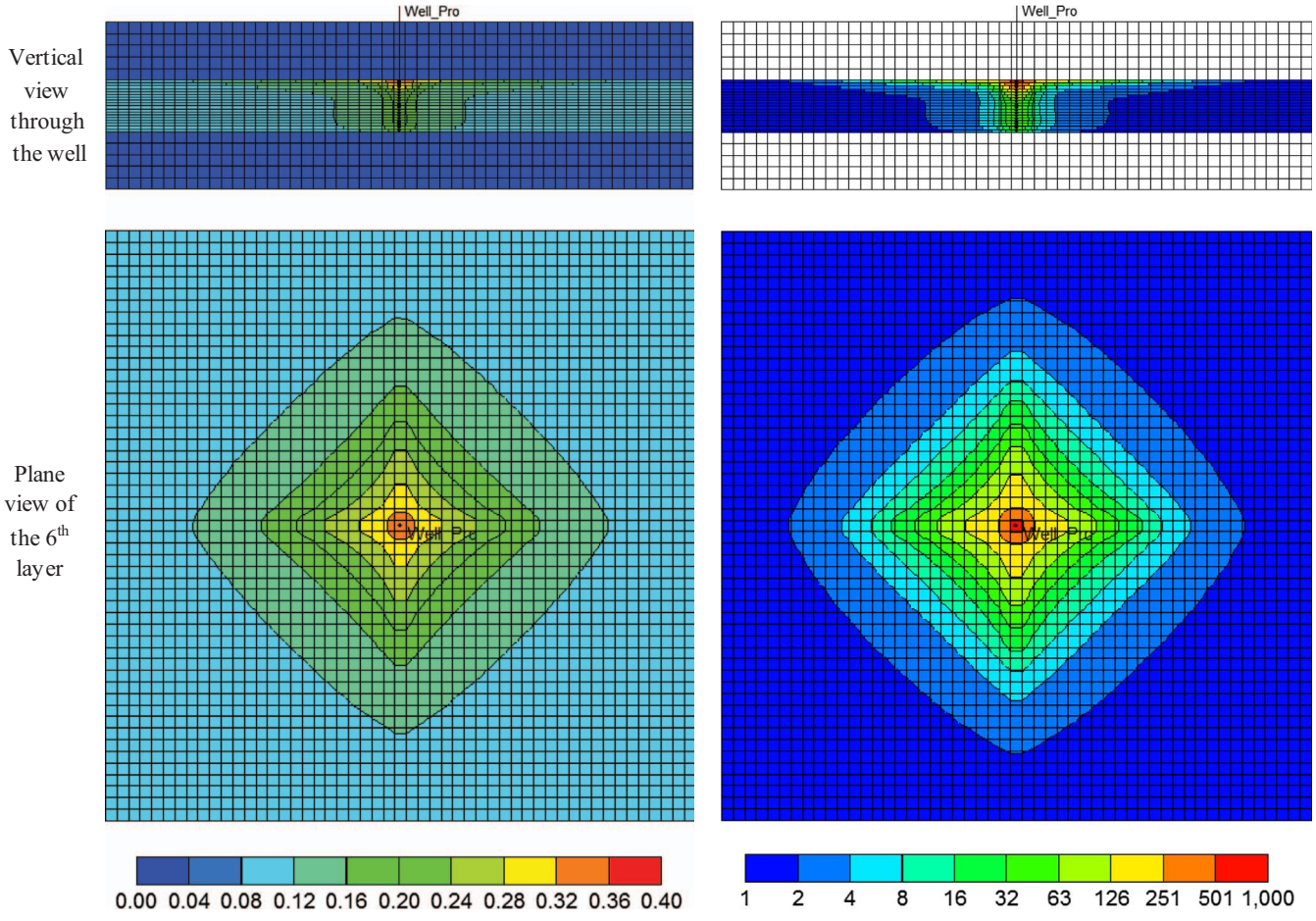

Fig. 9. Fluid porosity distribution at the end of the simulation.

Fig. 10. Effective permeability distribution at the end of the simulation (mD).

is about 25 m. The partial pressure of CH_4 in the gas phase changes greatly due to the introduction of substitute gas molecules, and the partial pressure of CH_4 in the near-wellbore area is lower than the equilibrium pressure, leading to the dissociation of the CH_4 hydrate. At the end of the simulation, the CH_4 hydrate saturation in the near-wellbore area decreased significantly (Fig. 7), and the CH_4 hydrate was highly dissociated in the upper part of the HBL, where the injected gas preferentially sweeps due to its smaller gravity compared with water. At the end of production, the dissociation percent [45] of the CH_4 hydrate is approximately 0.759%. The maximum radius of the significantly hydrate-dissociated area is about 20 m in the plane with an average value of 5 m. Therefore, the cyclic gas stimulation method can enhance the dissociation of the CH_4 hydrate, and the depressurization mechanism (partial pressure reduction) is dominant because the CO_2 hydrate formation is quite limited as discussed below.

The partial pressure change in CO_2 can also cause the dissociation and formation of the CO_2 hydrate. At the end of the simulation, a total of 33 556 m^3 (SCM) of gas mixture is injected, where 7550 m^3 is CO_2. Approximately 3.5% of CO_2 is stored in the reservoir (Tab. 7), and only a relatively small quantity of CO_2 hydrate is formed. The high-concentration CO_2 is mainly in the near-wellbore area, but cyclic production can cause near-wellbore pressure to rise and drop periodically each cycle which can affect CO_2 storage. On the other hand, the partial pressure of CO_2 in the gas phase is mostly lower than the equilibrium value during the cyclic production, and this is not beneficial for

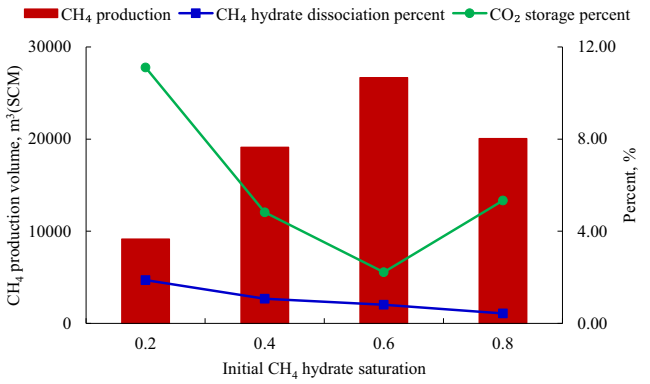

Fig. 11. Results of the sensitivity study of the initial CH_4 hydrate saturation.

CO_2 hydrate formation. Therefore, the cyclic production method may not effectively store CO_2, especially as a CO_2 hydrate.

3.2 Change of temperature, permeability and fluid porosity

During cyclic production stimulation, the CH_4 hydrate dissociation is dominant compared with the CO_2 hydrate formation, which can be inferred from the temperature distribution (Fig. 8), because the hydrate dissociation is an endothermic process. At the end of the simulation, the reservoir temperature decreases significantly with the maximum radius of 32 m, especially in the near-wellbore area where the lowest temperature approaches 1.5 °C. The similarity between the temperature distribution (Fig. 8) and the CH_4 hydrate concentration distribution (Fig. 7) shows that heat supply is quite essential for continuous hydrate dissociation. Besides the latent heat in the HBL, the latent heat contained in the overlying and bottom layers also plays an important part in the CH_4 hydrate dissociation (Fig. 8).

The effective permeability is the key factor affecting the pressure propagation, thus controlling the gas or water flow in the reservoir. It is correlated with the fluid porosity through equation (7), which is determined by the solid phase saturation, *i.e.* hydrate saturation. From Figures 9 and 10, the effective permeability and the fluid porosity of the hydrate reservoir increase significantly due to the CH_4 hydrate dissociation, with the highest permeability close to the reservoir absolute permeability (1D) and the highest fluid porosity close to the reservoir porosity (40%). This shows that the seepage condition improves as the production continues, and it is favorable for the water or gas flow in the hydrate reservoir during the injection or production stage.

3.3 Sensitivity analysis

The values of reservoir or operation parameters can have significant influence on the production performance of the hydrate reservoir. Using the base model, the sensitivity analyses of several parameters were conducted, including the initial CH_4 hydrate saturation, absolute permeability, intrinsic CO_2 hydrate formation rate constant, injected gas composition and production time.

Table 8. The effective permeability and injected/produced gas at the end of the simulation.

Initial CH_4 hydrate saturation	0.2	0.4	0.6	0.8
Average effective permeability, mD	303.92	72.71	11.25	0.60
Injected gas volume, m^3	35 500	34 800	33 985	19 730
Produced gas volume, m^3	40 720	52 235	59 904	38 700

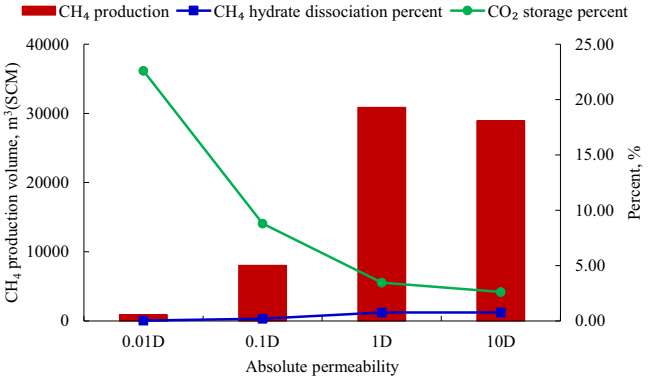

Fig. 12. Results of the sensitivity study of the absolute permeability.

3.3.1 Initial CH_4 hydrate saturation

The initial CH_4 hydrate saturation value was set to 0.2, 0.4, 0.6 and 0.8. From Figure 11, the CH_4 production volume increases when the initial CH_4 hydrate saturation increases from 0.2 to 0.6, but the CH_4 hydrate dissociation percent and the CO_2 storage percent decrease. The production is dominated by the reserve (CH_4 hydrate saturation), but a high CH_4 hydrate saturation is not helpful for CO_2 storage due to low gas injectivity (Tab. 8). When the saturation value changes to 0.8, the influence of the poor seepage condition is more significant, and the CH_4 production volume and the total amount of injected gas decrease.

3.3.2 Absolute permeability

The absolute permeability was set to 0.01, 0.1, 1 and 10 D, and the results are shown in Figure 12. With the increase in the absolute permeability, the CH_4 production volume and the CH_4 hydrate dissociation percent increase due to the improvement of the seepage condition, while the CO_2 storage percent decreases significantly.

However, when the permeability increases to 10 D, the CH_4 production will decrease. This is because when the absolute permeability value is too high (10 D for example), the injected gas will mainly accumulate in the upper part of

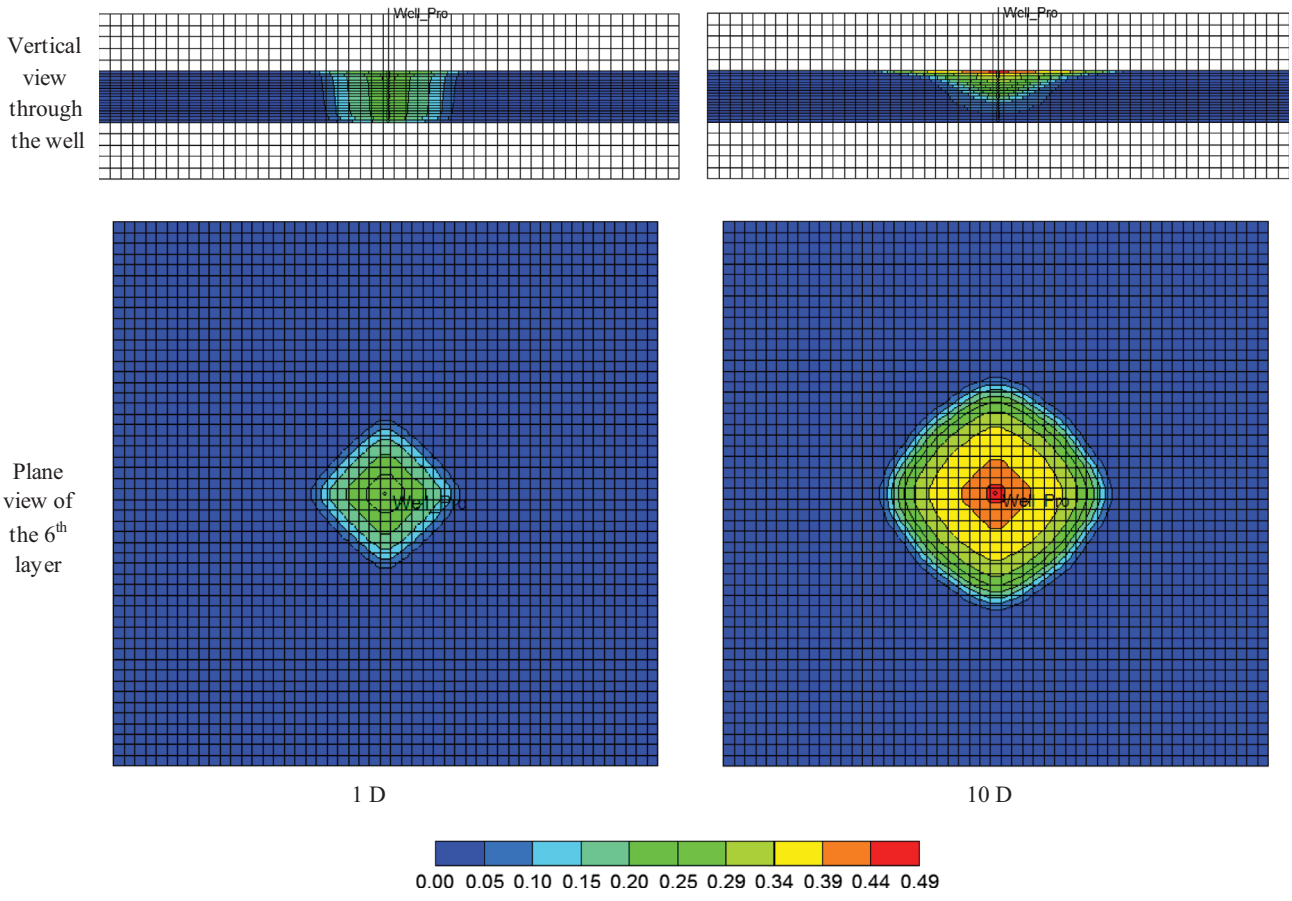

Fig. 13. Gas saturation distribution at the end of the gas injection period of the 1st cycle.

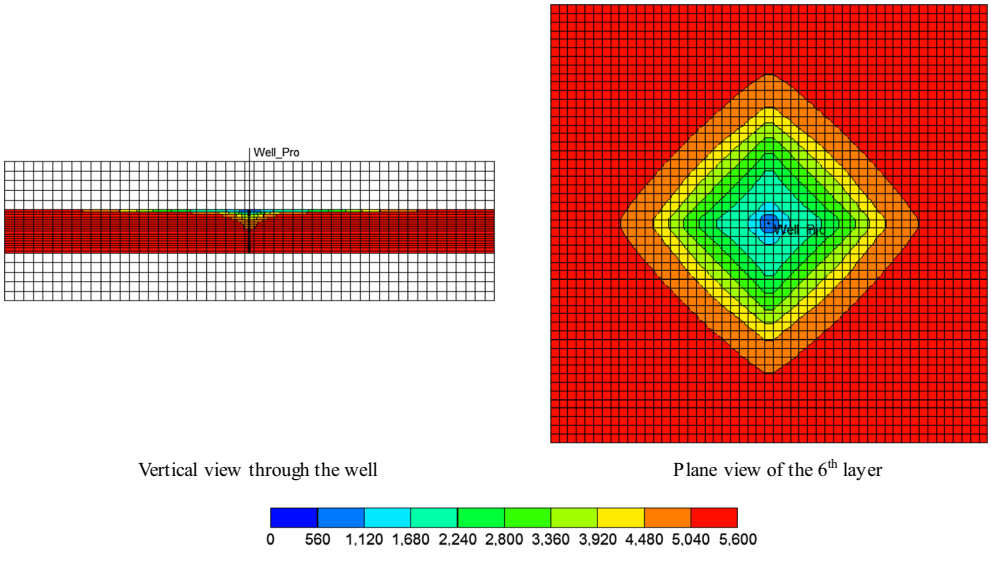

Fig. 14. CH_4 hydrate concentration at the end of the simulation when the absolute permeability is 10 D (mol/m^3).

Table 9. The values of the heterogeneity.

Reservoir parameters	HBL	Scheme 1 (negative rhythm)	Scheme 2 (homogeneous)	Scheme 3 (positive rhythm)
Absolute permeability, D	Top layer	1.5	1.0	0.5
	Middle layer	1.0	1.0	1.0
	Bottom layer	0.5	1.0	1.5

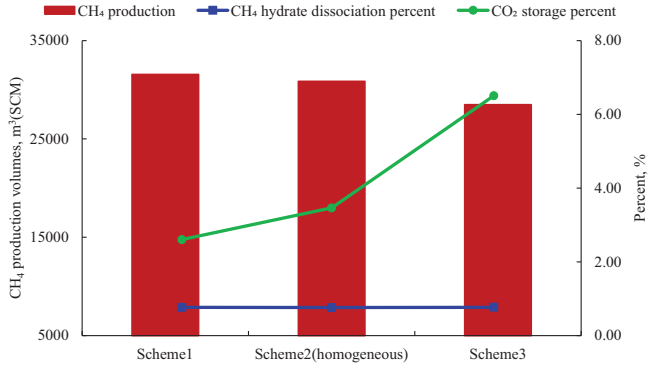

Fig. 15. Results of the sensitivity study of the vertical heterogeneity of the absolute permeability.

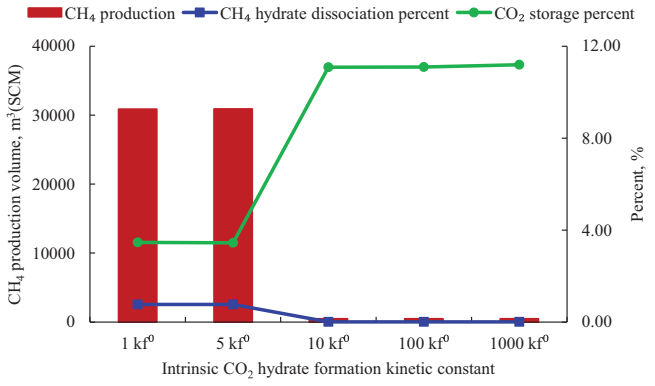

Fig. 17. Results of the sensitivity study of the intrinsic CO_2 hydrate formation kinetic constant.

the hydrate reservoir because of its lower gravity, which limits its effect in enhancing the CH_4 production. Taking the 1st cycle for an example (Fig. 13), the total sweeping volume of the injected gas is more uniform and larger at the end of gas injection when the absolute permeability is 1 D. Thus, the dissociation region of the CH_4 hydrate is larger in the plane but smaller in the vertical area (Fig. 14) compared with the situation of 1 D (Fig. 7). The overall dissociation region of the CH_4 hydrate is limited when the absolute permeability is 10 D, resulting in a decline in CH_4 production.

3.3.3 Heterogeneity of absolute permeability

To investigate the influence of the vertical heterogeneity of the absolute permeability. Three situations are considered, *i.e.* scheme 1 (negative rhythm), scheme 2 (homogeneous), and scheme 3 (positive rhythm), as shown in Table 9. For scheme 1, the value of the absolute permeability increases from the top layer to the bottom layer of the HBL, and scheme 3 is just the opposite. The results of the sensitivity studies are shown in Figure 15.

From Figure 15, for the CH_4 production, scheme 1 is the best, followed by scheme 2 and scheme 3 in sequence. This is because the injected gas prefers to accumulate in the upper layer of the hydrate reservoir, and high permeability can assist the injected gas to take effect to increase the CH_4 production, as shown in Figure 16. From Figure 16, however, the CH_4 hydrate dissociation area is more uniform in scheme 3 than in scheme 1. That is, the negative rhythm is the most preferred scheme for CH_4 production, but the least preferred one for CO_2 storage.

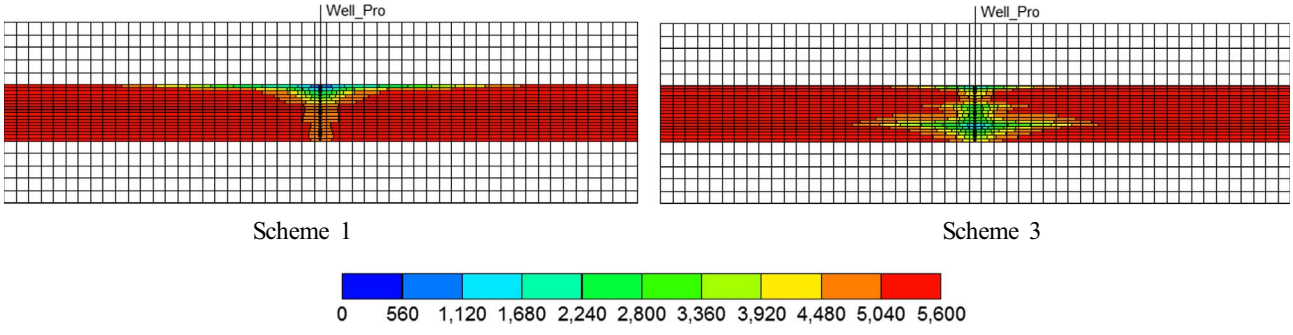

Fig. 16. CH_4 hydrate concentration at the end of the simulation from vertical view through the well (mol/m^3).

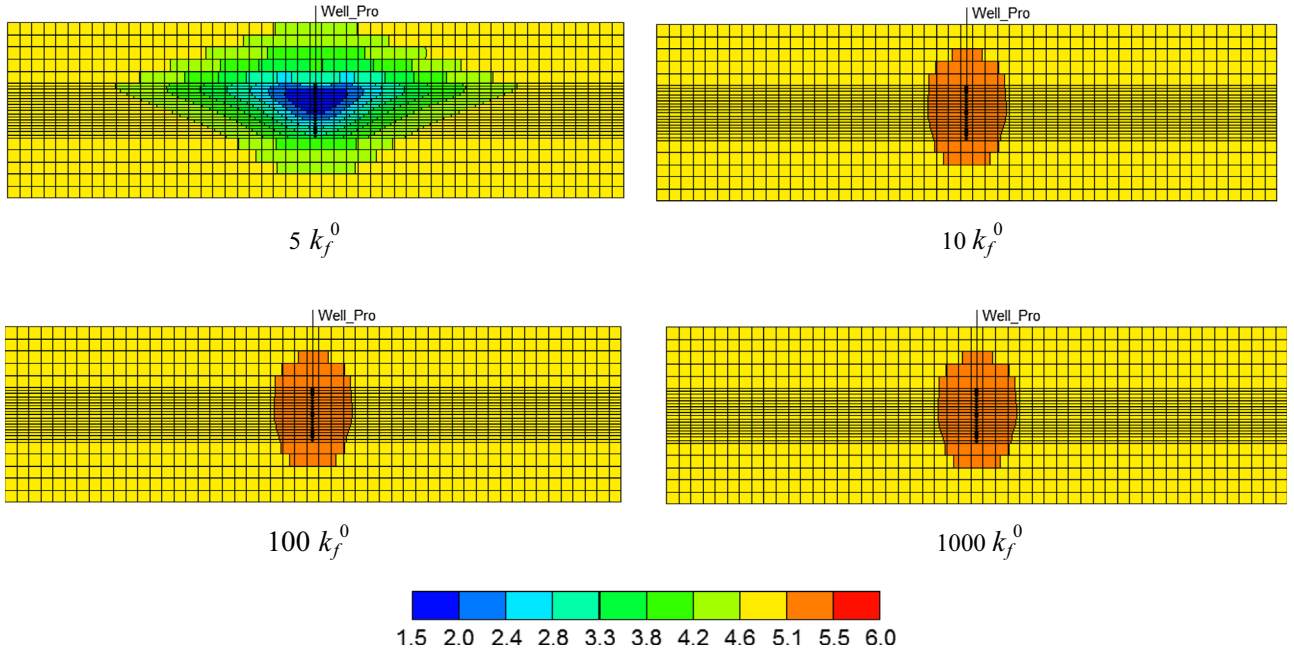

Fig. 18. Temperature distribution at the end of the simulation (vertical view through the well, °C).

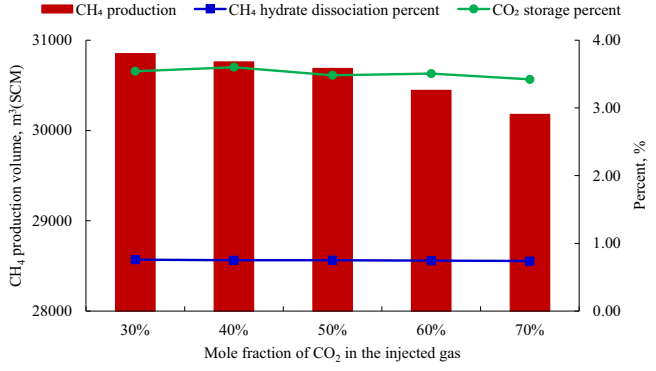

Fig. 19. Results of the sensitivity study of the injected gas composition.

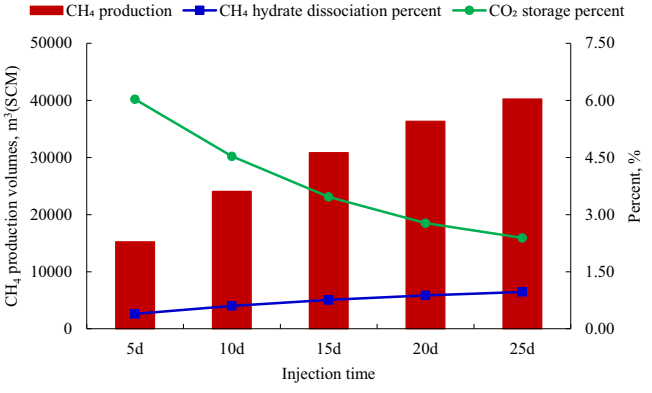

Fig. 21. Results of the sensitivity study of the injection time.

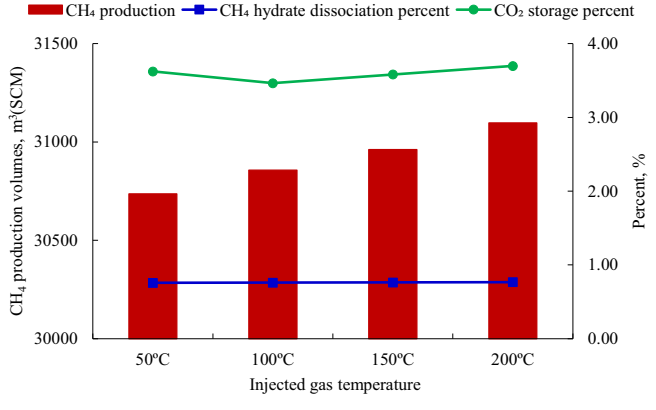

Fig. 20. Results of the sensitivity study of the injected gas composition.

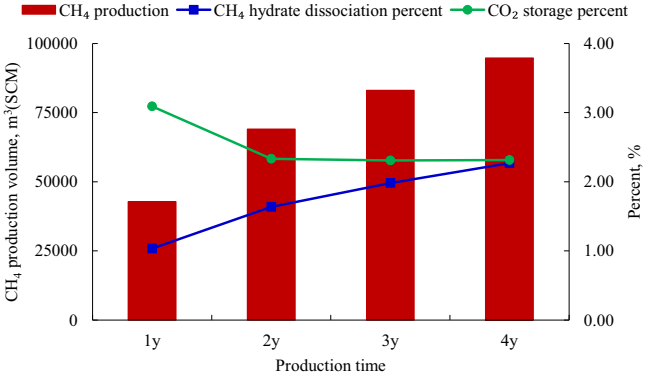

Fig. 22. Results of the sensitivity study of the production time.

3.3.4 Intrinsic CO_2 hydrate formation kinetic constant

The parameter values of hydrate kinetics are taken from bulk phase systems in this paper because these values are less accessible in porous media [46–48]. Besides, the measurement of the hydrate formation kinetic constant is much more difficult, which also exhibits a weak correlation to the temperature [49, 50]; thus, there is great uncertainty. For the reasons presented above, we carried out the sensitivity study on the intrinsic CO_2 hydrate formation kinetic constant.

The intrinsic CO_2 hydrate formation kinetic constant was set to 5, 10, 100 and 1000 k_f^0, where k_f^0 is the value in the base model. The high CO_2 hydrate formation kinetic constant is unfavorable for hydrate production but favorable for CO_2 storage (Fig. 17), especially when it is higher than 10 k_f^0. This trend is observed because as the CO_2 hydrate formation kinetic constant increases, the CO_2 hydrate quick formation in the near-wellbore area weakens the CH_4 hydrate dissociation. The CO_2 hydrate formation degree is more significant than the CH_4 hydrate dissociation, and this can be deduced from the temperature distribution of Figure 18.

3.3.5 Injected gas composition

The CO_2 mole fraction in the injected gas was set to 0.3, 0.4, 0.5, 0.6 and 0.7, and the results are shown in Figure 19. The injected gas composition has little effect on the CH_4 hydrate dissociation percent and CO_2 storage percent. This result is observed because in the established model, there is no essential difference in the role of the pressure reduction by CO_2 and N_2, as there is only a small amount of CO_2 hydrate formed. The CH_4 production volume slightly decreases with the increase of the CO_2 mole fraction in the injected gas, because these small-amount formed CO_2 hydrate may influence the seepage condition. From this aspect, smaller CO_2 mole fraction in the mixture is more beneficial to the CH_4 production, and pure N_2 can have the best production performance.

3.3.6 Injected gas temperature

The injected gas temperature was set to 50, 100, 150 and 200 °C, and the results are shown in Figure 20. The CH_4 hydrate dissociation percent and CO_2 storage percent vary little with the injected gas temperature. The CH_4 production volume slightly increases with the increase of the gas temperature. This is because the injected gas conveys a small amount of heat due to its low heat capacity, and the latent heat contained in the reservoir provides the most consumed heat for the CH_4 hydrate dissociation.

3.3.7 Injection time

The injection time of each cycle was set to 5, 10, 15, 20 and 25 days. From Figure 21, a longer injection time can enhance the CH_4 production volume and the CH_4 hydrate dissociation percent. More gas will be injected into the reservoir as the injection time increases, and this can induce more hydrate to dissociate. The CH_4 production volume increases about 164% as the injection time increases from 5 days to 25 days, but the increase of the CH_4 production slows down when the injection time is beyond 15 days. However, longer injection time is unfavorable for CO_2 storage and the CO_2 storage percent decreases from 6.03% to 2.39% as the injection time increases from 5 days to 25 days.

3.3.8 Production time

The production time was set to 1, 2, 3 and 4 years. From Figure 22, a longer production time can enhance the CH_4 production volume and the CH_4 hydrate dissociation percent. After a four-year production, about 2.27% of the CH_4 hydrate has been dissociated compared to the dissociation percent of 1.03% after a one-year production. The CO_2 storage percent will decrease to a stable low level as the production time increases.

4 Summary and conclusion

This paper proposed the cyclic methane hydrate production method with CO_2 and N_2 mixture stimulation, and investigated the field-scale production using this method based on a numerical model according to actual hydrate reservoir parameters. The following conclusions were obtained:

1. The depressurization mechanism is dominant in cyclic stimulation with the CO_2 and N_2 mixture; in addition, the CH_4 hydrate can be significantly produced due to the effective reduction of the partial pressure of CH_4 in the gas phase, and the CH_4 hydrate in the upper part of the HBL is highly dissociated. However, the effect of CO_2 storage is limited, and a continuous CO_2 injection (*i.e.*, CO_2 flooding) may be better for CO_2 storage. The waste gas produced from the plant (mainly composed of CO_2 and N_2) may be directly injected into the hydrate reservoir for production.
2. In the near-wellbore area, the hydrate dissociation degree is relatively high, and the fluid porosity and effective permeability increase significantly during the cyclic stimulation process. Heat supply plays an important role in the cyclic production. The reservoir temperature decreases significantly, and the overlying and bottom layers can supply some heat for CH_4 hydrate dissociation in addition to the HBL. External heat can be added to improve the hydrate reservoir production during the process.
3. Relatively high initial CH_4 hydrate saturation, high reservoir absolute permeability, and long injection or production time are helpful in improving the CH_4 hydrate production; however, they are adverse to CO_2 storage. Too high of an initial CH_4 hydrate saturation or reservoir absolute permeability will cause a decrease in the CH_4 production due to poor seepage conditions. Relatively speaking, the injected gas temperature and injected gas composition have limited effect on the CH_4 hydrate production or CO_2 storage.

5 Comments

The findings in this paper are based on the model established from publicly available data; however, some parameter values may not be quite accurate, especially in the porous media environment, which may have a significant influence on the results. For example, the hydrate formation kinetics are not easy to determine, and do not follow an Arrhenius temperature dependence. Moreover, the dissolution of CO_2 into the aqueous phase probably has some influence on the simulation results. However, this study can provide some insights into the cyclic CH_4 hydrate production process.

Acknowledgments. This work was supported by the School-Level Scientific Research of Shengli College, China University of Petroleum (Grant No. KY2018018), the Important National Science and Technology Specific Projects of China (Grant No. 2017ZX05013-001), and the Youth Innovation Team Science and Technology Development Program of Shandong Province Higher Educational Institutions (Grant No. 2019KJA024).

References

1 Sloan E.D. (2008) *Clathrate hydrates of natural gases*, CRC Press, USA.
2 Li X.S., Xu C.G., Zhang Y., Ruan X.K., Li G., Wang Y. (2016) Investigation into gas production from natural gas hydrate: A review, *Appl. Energy* **172**, 286–322.
3 Bai Y., Yang H., Du Y., Zhao Y. (2013) The sensitivity analysis of scaling criteria in gas hydrate reservoir physical simulation, *Energy Convers. Manage.* **67**, 138–144.
4 Zhao J., Liu D., Yang M., Song Y.C. (2014) Analysis of heat transfer effects on gas production from methane hydrate by depressurization, *Int. J. Heat Mass Transfer* **77**, 529–541.
5 Feng Y., Chen L., Suzuki A., Kogawa T., Okajima J., Komiya A., et al. (2019) Enhancement of gas production from methane hydrate reservoirs by the combination of hydraulic fracturing and depressurization method, *Energy Convers. Manage.* **184**, 194–204.
6 Xia Z., Wang X., Zhang X. (2020) Investigation of the hydrate reservoir production under different depressurization modes, *Mar. Georesour. Geotechnol.* **38**, 8, 1002–1012.
7 Kurihara M., Sato A., Funatsu K., Ouchi H., Yamamoto K., Numasawa M., Ebinuma T., Narita H., Masuda Y., Dallimore S.R., Wright F., Ashford D. (January 1 2010) Analysis of production data for 2007/2008 Mallik gas hydrate production tests in Canada, *International Oil and Gas Conference and Exhibition in China*, Society of Petroleum Engineers, pp. 1–24.
8 Yamamoto K., Terao Y., Fujii T., Ikawa T., Seki M., Matsuzawa M., Kanno T. (2014) Operational overview of the first offshore production test of methane hydrates in the Eastern Nankai Trough, *Offshore Technology Conference*, Society of Petroleum Engineers, pp. 1–11.
9 Li J., Ye J., Qin X., Qiu H., Wu N., Lu H., et al. (2018) The first offshore natural gas hydrate production test in South China Sea, *China Geology* **1**, 1, 5–16.
10 Myshakin E.M., Gaddipati M., Rose K., Anderson B.J. (2012) Numerical simulations of depressurization-induced gas production from gas hydrate reservoirs at the Walker Ridge 313 site, northern Gulf of Mexico, *Mar. Pet. Geol.* **34**, 1, 169–185.
11 Sun Y., Ma X., Guo W., Jia R., Li B. (2019) Numerical simulation of the short- and long-term production behavior of the first offshore gas hydrate production test in the South China Sea, *J. Pet. Sci. Eng.* **181**, 1–13.
12 Yu T., Guan G., Abudula A., Yoshida A., Wang D., Song Y. (2019) Gas recovery enhancement from methane hydrate reservoir in the Nankai Trough using vertical wells, *Energy* **166**, 834–844.
13 Ohgaki K., Takano K., Sangawa H., Matsubara T., Nakano S. (1996) Methane exploitation by carbon dioxide from gas hydrates – phase equilibria for CO_2-CH_4 mixed hydrate system, *J. Chem. Eng. Jpn.* **29**, 3, 478–483.
14 Lee Y., Choi W., Shin K., Seo Y. (2017) CH_4-CO_2 replacement occurring in sII natural gas hydrates for CH_4 recovery and CO_2 sequestration, *Energy Convers. Manage.* **150**, 356–364.
15 Gharasoo M., Babaei M., Haeckel M. (2019) Simulating the chemical kinetics of CO_2-methane exchange in hydrate, *J. Natural Gas Sci. Eng.* **62**, 330–339.
16 Shagapov V.S., Khasanov M.K., Musakaev N.G., Duong N. H. (2017) Theoretical research of the gas hydrate deposits development using the injection of carbon dioxide, *Int. J. Heat Mass Trans.* **107**, 347–357.
17 Khasanov M.K., Stolpovsky M.V., Gimaltdinov I.K. (2019) Mathematical model of injection of liquid carbon dioxide in a reservoir saturated with methane and its hydrate, *Int. J. Heat Mass Trans.* **132**, 529–538.
18 Koh D.-Y., Ahn Y.-H., Kang H., Park S., Lee J.Y., Kim S.-J., Lee J., Lee H. (2015) One-dimensional productivity assessment for on-field methane hydrate production using CO_2/N_2 mixture gas, *AIChE J.* **61**, 3, 1004–1014.
19 Yang J., Okwananke A., Tohidi B., Chuvilin E., Maerle K., Istomin V., Bukhanov B., Cheremisin A. (2017) Flue gas injection into gas hydrate reservoirs for methane recovery and carbon dioxide sequestration, *Energy Convers. Manage.* **136**, 431–438.
20 Li B., Xu T., Zhang G., Guo W., Liu H., Wang Q., et al. (2018) An experimental study on gas production from fracture-filled hydrate by CO_2 and CO_2/N_2 exchange, *Energy Convers. Manage.* **165**, 738–747.
21 Sun Y.F., Wang Y.F., Zhong J.R., Li W.Z., Li R., Cao B.J., Kan J.Y., Sun C.Y., Chen G.J. (2019) Gas hydrate exploitation using CO_2/H_2 mixture gas by semi-continuous injection-production mode, *Appl. Energy* **240**, 215–225.
22 Merey S., Al-Raoush R.I., Jung J., Alshibli K.A. (2018) Comprehensive literature review on CH_4-CO_2 exchange in microscale porous media, *J. Pet. Sci. Eng.* **171**, 48–62.
23 Okwananke A., Yang J., Tohidi B., Chuvilin E., Istomin V., Bukhanov B., Cheremisin A. (2018) Enhanced depressurization for methane recovery from gas hydrate reservoirs by injection of compressed air and nitrogen, *J. Chem. Thermodyn.* **117**, 138–146.
24 Boswell R., Schoderbek D., Collett T.S., Ohtsuki S., White M., Anderson B.J. (2016) The Ignik Sikumi field experiment, Alaska North Slope: design, operations, and implications for CO_2–CH_4 exchange in gas hydrate reservoirs, *Energy Fuels* **31**, 1, 140–153.
25 Hou J., Xia Z., Li S., Zhou K., Lu N. (2016) Operation parameter optimization of a gas hydrate reservoir developed by cyclic hot water stimulation with a separated-zone horizontal well based on particle swarm algorithm, *Energy* **96**, 581–591.

26 CMG STARS® (2010) *Advanced process and thermal reservoir simulator*, Computer Modelling Group Ltd., Calgary, Alberta, Canada.

27 Anderson B.J., Kurihara M., White M.D., Moridis G.J., Wilson S.J., Pooladi-Darvish M., Gaddipati M., Masuda Y., Collett T.S., Hunter R.B., Narita H., Rose K., Boswell R. (2011) Regional long-term production modeling from a single well test, Mount Elbert gas hydrate stratigraphic test well, Alaska North slope, *Mar. Pet. Geol.* **28**, 2, 493–501.

28 Giraldo C., Klump J., Clarke M., Schicks J. (2014) Sensitivity analysis of parameters governing the recovery of methane from natural gas hydrate reservoirs, *Energies* **7**, 4, 2148–2176.

29 Walsh M.R., Hancock S.H., Wilson S.J., Patil S.L., Moridis G. J., Boswell R., Collett T.S., Koh C.A., Sloan E.D. (2009) Preliminary report on the commercial viability of gas production from natural gas hydrates, *Energy Econ.* **31**, 5, 815–823.

30 Zatsepina O., Pooladi-Darvish M., Hong H. (2011) Behavior of gas production from Type III hydrate reservoirs, *J. Natural Gas Sci. Eng.* **3**, 3, 496–504.

31 Zatsepina O., Pooladi-Darvish M. (2012) Storage of CO_2 as hydrate in depleted gas reservoirs, *SPE Reserv. Evalu. Eng.* **15**, 1, 98–108.

32 Hou J., Ji Y., Zhou K., Liu Y., Wei B. (2018) Effect of hydrate on permeability in porous media: Pore-scale microsimulation, *Int. J. Heat Mass Transfer* **126**, 416–424.

33 White M.D., Wurstner S.K., McGrail B.P. (2011) Numerical studies of methane production from Class 1 gas hydrate accumulations enhanced with carbon dioxide injection, *Mar. Pet. Geol.* **28**, 2, 546–560.

34 Anderson B., Boswell R., Collett T.S., Farrell H., Ohtsuki S., White M. (2014) *Review of the findings of the Iġnick Sikumi CO_2-CH_4 gas hydrate exchange field trial*, Society of Petroleum Engineers, pp. 1–11.

35 Myshakin E.M., Ajayi T., Anderson B.J., Seol Y., Boswell R. (2016) Numerical simulations of depressurization-induced gas production from gas hydrates using 3-D heterogeneous models of L-Pad, Prudhoe Bay Unit, North Slope Alaska, *J. Natural Gas Sci. Eng.* **35**, 1336–1352.

36 Kang S.P., Lee H., Ryu B.J. (2001) Enthalpies of dissociation of clathrate hydrates of carbon dioxide, nitrogen, (carbon dioxide + nitrogen), and (carbon dioxide + nitrogen + tetrahydrofuran), *J. Chem. Thermodyn.* **33**, 5, 513–521.

37 Kim H.C., Bishnoi P.R., Heidemann R.A., Rizvi S.S. (1987) Kinetics of methane hydrate decomposition, *Chem. Eng. Sci.* **42**, 7, 1645–1653.

38 Yin Z., Chong Z.R., Tan H.K., Linga P. (2016) Review of gas hydrate dissociation kinetic models for energy recovery, *J. Natural Gas Sci. Eng.* **35**, 1362–1387.

39 Shahbazi A. (2010) Mathematical modeling of gas production from gas hydrate reservoirs, *PhD Thesis*, University of Calgary, Canada.

40 Uddin M., Coombe D., Law D., Gunter B. (2008) Numerical studies of gas hydrate formation and decomposition in a geological reservoir, *J. Energy Resour. Technol.* **130**, 3, 1–14.

41 Clarke M., Bishnoi P.R. (2001) Determination of the activation energy and intrinsic rate constant of methane gas hydrate decomposition, *Can. J. Chem. Eng.* **79**, 1, 143–147.

42 Clarke M., Bishnoi P.R. (2004) Determination of the intrinsic rate constant and activation energy of CO_2 gas hydrate decomposition using in-situ particle size analysis, *Chem. Eng. Sci.* **59**, 14, 2983–2993.

43 Adisasmito S., Frank R.J. III, Sloan E.D. Jr (1991) Hydrates of carbon dioxide and methane mixtures, *J. Chem. Eng. Data* **36**, 1, 68–71.

44 Collett T.S., Boswell R., Lee M.W., Anderson B.J., Rose K., Lewis K.A. (2012) Evaluation of long-term gas-hydrate-production testing locations on the Alaska North Slope, *SPE Reserv. Eval. Eng.s* **15**, 2, 243–264.

45 Xia Z., Hou J., Liu Y., Li S., Du Q., Lu N. (2017) Production characteristic investigation of the Class I, Class II and Class III hydrate reservoirs developed by the depressurization and thermal stimulation combined method, *J. Pet. Sci. Eng.* **157**, 56–67.

46 Uchida T., Ebinuma T., Takeya S., Nagao J., Narita H. (2002) Effects of pore sizes on dissociation temperatures and pressures of methane, carbon dioxide, and propane hydrates in porous media, *J. Phys. Chem. B* **106**, 4, 820–826.

47 de Lima Silva P.H., Naccache M.F., de Souza Mendes P.R., Teixeira A., Valim L.S. (2020) Rheology of THF hydrate slurries at high pressure, *Oil Gas Sci. Technol. – Rev IFP Energies Nouvelles* **75**, 16.

48 Kiran B.S., Sowjanya K., Prasad P.S.R., Yoon J.H. (2019) Experimental investigations on tetrahydrofuran–methane–water system: Rapid methane gas storage in hydrates, *Oil Gas Sci. Technol. – Rev. IFP Energies Nouvelles* **74**, 12.

49 Malegaonkar M.B., Dholabhai P.D., Bishnoi P.R. (1997) Kinetics of carbon dioxide and methane hydrate formation, *Can. J. Chem. Eng.* **75**, 6, 1090–1099.

50 Sun X. (2005) Modeling of hydrate formation and dissociation in porous media. *PhD Thesis*, University of Houston, USA.